ISSN 0021-3640, JETP Letters, 2019, Vol. 109, No. 3, pp. 175–179. © Pleiades Publishing, Inc., 2019.

CONDENSED MATTER

Vapor-Phase Synthesis and Magnetoresistance of $(Cd_{0.993}Zn_{0.007})_3As_2$ Single Crystals[1]

A. V. Kochura[a], L. N. Oveshnikov[b, c, *], A. P. Kuzmenko[a], A. B. Davydov[c], S. Yu. Gavrilkin[c], V. S. Zakhvalinskii[d], V. A. Kulbachinskii[b, e, f], N. A. Khokhlov[a], and B. A. Aronzon[c]

[a] *Southwest State University, Kursk, 305040 Russia*

[b] *National Research Center Kurchatov Institute, Moscow, 123182 Russia*

[c] *Lebedev Physical Institute, Russian Academy of Sciences, Moscow, 119991 Russia*

[d] *Belgorod National Research University, Belgorod, 308015 Russia*

[e] *Moscow State University, Moscow, 119991 Russia*

[f] *Moscow Institute of Physics and Technology (State University), Dolgoprudnyi, Moscow region, 141700 Russia*

**e-mail: Oveshln@gmail.com*

Received November 27, 2018; revised November 27, 2018; accepted November 28, 2018

We report a highly anisotropic magnetoresistance of $(Cd_{0.993}Zn_{0.007})_3As_2$ single crystals, which have been synthesized by the vapor-phase growth. Scanning electron microscopy and electron diffraction data confirm the high crystalline quality of obtained samples. Studied samples exhibit specific features such as octahedral nuclei growth and step-like morphology of the surface formed by {112} planes. The giant anisotropic magnetoresistance and Shubnikov–de Haas oscillations have been observed at low temperatures. The results suggest the existence of the Dirac semimetal phase in $(Cd_{1-x}Zn_x)_3As_2$ solid solution with low zinc content. Thus, the observed magnetoresistance anisotropy is partially attributed to the chiral anomaly.

DOI: 10.1134/S0021364019030019

Further advancement of modern technologies in many respects depends on the materials with fundamentally new properties. The Dirac and Weyl semimetals (DSM and WSM) are considered as such materials, having a tremendous potential for applications [1]. A key feature of these semimetals is their inverted band structure, which yield a set of isolated points within the Brillouin zone, where conduction and valence bands contact each other. The gapless electronic states near these symmetry-protected Dirac points have linear dispersion and rigidly coupled spin and momentum directions. The exact spin structure of such states is characterized by their chirality ($C = \pm 1$). A DSM system have even number of Dirac points and doubly degenerate bands (chiral degeneracy). These systems are considered as a 3D graphene analogue, and therefore they are of considerable interest for both fundamental science and applications.

Among numerous materials that were theoretically predicted to manifest DSM phase, only few ones actually exhibit nontrivial properties characteristic of DSM systems. Cd_3As_2 single crystal is one of such systems. Various effects were experimentally discovered for Cd_3As_2, including the Shubnikov–de Haas (SdH) oscillations with nontrivial phase [2], giant linear magnetoresistance [3, 4], photovoltaic effect from Cd_3As_2 nanoplate/metal contacts [5], and nontrivial photoelectromagnetic effect [6]. An extremely high mobility of charge carriers in Cd_3As_2 and ultrafast photocurrent response (6.9 ps) [7] make this material to be highly promising for the usage in electronic devices, including those operating within the terahertz range [7, 8].

Although the number of papers dealing with DSMs is rapidly increasing, such studies are currently only at an early stage. In this field of research, one encounters with certain difficulties. One of them is a high defect formation rate during the growth of Cd_3As_2 crystals. Defects create crystal structure distortions and lead to an increase in the charge carrier density. The specific features of DSM are most pronounced if the Fermi level is located near the Dirac point. The doping can compensate some negative features introduced by defects and even give rise to new useful characteristics. Therefore, the studies of Cd_3As_2-based solid solutions in the form of single crystals provide a deeper insight into the topological phases in similar materials and help in finding out the conditions for their applications. In this work, we describe the peculiarities of magnetotransport properties and analyze the struc-

[1] The article is published in the original.

tural characteristics of $(Cd_{0.993}Zn_{0.007})_3As_2$ single crystal grown by vapor-phase method.

Polymorphism is a characteristic feature of the Cd_3As_2 compound, which may crystallize in four modifications: α (space group $I4_1cd$), α' (space group $P4_2/nbc$), α'' (space group $P4_2/nmc$), and β (space group $P4_232$). The α modification occurs at the lowest temperatures, whereas β is the modification arising at the highest temperatures. The sequence of structural phase transitions occurring in Cd_3As_2 corresponds to the following scheme: α-Cd_3As_2 → 503 K → α'-Cd_3As_2 → 738 K → α''-Cd_3As_2 → 868 K → β-Cd_3As_2 [9]. In $(Cd_{1-x}Zn_x)_3As_2$ with $0.45 < x < 0.74$, an additional α''' (space group $I4_1/amd$) appears near the room temperature [9, 10].

Conventional melt crystallization (Bridgman–Stockbarger, Czochralski, and high thermal gradient directional solidification) techniques are not suitable for the growth of high-quality $(Cd_{1-x}Zn_x)_3As_2$ single crystals due to the β → α'' phase transition, which leads to the formation of structural defects and to the increase in the charge carrier density up to 10^{17}–10^{18} cm^{-3}. Fortunately, electron density in Cd_3As_2 can be diminished down to 10^{15}–10^{16} cm^{-3} by a compensation doping [11, 12]. At the same time, Cd_3As_2 crystals grown from the vapor phase at deposition temperatures below the β → α'' transition temperature demonstrate higher crystalline quality and high mobility of charge carriers (9×10^6 $cm^2/(V\,s)$ at $T = 5$ K [13]). Thus, we decided to use vapor-phase method [14] to grow $(Cd_{1-x}Zn_x)_3As_2$ single crystals studied in this work.

The Cd_3As_2 powder, pre-cleaned by the vacuum sublimation, and Zn powder were loaded into long borosilicate glass vial. Then, the vial was pumped out to the pressure of 10^{-5} mm Hg, sealed, and placed into the two-zone furnace with temperatures of the evaporation and deposition zones being within ranges of 520–600°C and 450–500°C, respectively. The Cd_3As_2 powder was located within the evaporation zone and the zinc – within the deposition zone. The growth of $(Cd_{1-x}Zn_x)_3As_2$ single crystals occurs in the deposition zone.

The microstructure of the samples was studied using a scanning electron microscope (SEM) (JSM-6610LV, Jeol, Japan) equipped with a microanalyzer (X-Max^N, Oxford Instruments, United Kingdom, 0.1% surface elemental analysis precision) for energy-dispersive X-ray spectroscopy (EDXS). The chemical composition of the samples was calculated based on the X-ray emission spectra. Secondary and backscattered electron detectors were used. The transmission electron microscope (JEM-2100, Jeol, Japan) was used for obtaining the electrographic images. Raman spectra were measured at room temperature with a confocal microscope (OmegaScope^{TM}, AIST-NT Inc., United States, excitation wavelength 532 nm, power 50 mW, focused light spot size about 500 nm, 0.8 cm^{-1} spectral resolution). Transport properties were studied by the four-point probe method employing an automated measurement system (PPMS-9, Quantum Design, United States). The measurements were carried out by the ac method using rectangular current pulses with the repetition rate of 8 Hz at magnetic fields up to 9 T. Two magnetic field orientations were used: (i) perpendicular to the sample holder, denoted as $B_\perp$, and (ii) parallel to the sample holder and hence to the current direction, denoted as $B_\parallel$.

Crystals $(Cd_{1-x}Zn_x)_3As_2$ form a continuous range ($0 \le x \le 1$) of solid solutions. In these solid solutions, the bandgap (at liquid helium temperatures) gradually changes from about −0.1 eV ($x = 0$) to 1.07 eV ($x = 1$) with a linear law [15]. The DSM-semimetal transition occurs at some doping level x_c. However, the data concerning the value of x_c are quite ambiguous. For the samples grown from the vapor phase, the study of photoelectromagnetic effect suggests that the transition occurs at $0.045 < x < 0.25$ [6]. Nevertheless, magnetotransport measurements for crystals produced by melt crystallization techniques demonstrated that $x_c \approx 0.38$ [16]. This discrepancy stimulates further investigations of the DSM-semimetal transition in $(Cd_{1-x}Zn_x)_3As_2$ compound. The structure of the crystals with low Zn content should demonstrate higher quality than that of undoped Cd_3As_2 crystals, while they should also maintain the DSM properties as well. We have chosen the sample with the lowest Zn content. For it, the EDXS gives the composition around $x \approx 0.007$ (Fig. 1): 0.42 at % Zn, 59.38 at % Cd, and 40.2 at % As.

The electron diffraction pattern shown in Fig. 1a demonstrated high crystalline quality of the sample and the absence of defects related to the Zn doping. The crystal lattice was found to be tetragonal with parameters $a = 12.7$ Å and $c = 25.4$ Å (which agrees well with $a = 12.6461$ Å and $c = 25.4378$ Å for α-Cd_3As_2 [9]). We have found signatures of nucleation process at the sample surface. The nuclei had the octahedron shape with the sizes of about 1 μm (Fig. 1b). It was shown earlier [5], that such octahedra are formed in the nanostructures of Cd_3As_2 during the synthesis from the vapor phase. In this case, the [001] lattice direction turns out to be along the main octahedron diagonal, whereas the side faces are formed by {112} planes. The [112] direction is the most favorable in the growth of Cd_3As_2 single crystals since the surface free energy of the (112) face has the minimum value as compared to the energies of the other faces, whereas the average distance between the atomic layers along the [112] direction is higher (7.3 Å) [17]. Therefore, the {112} plane is the natural chip plane for α-Cd_3As_2 sin-

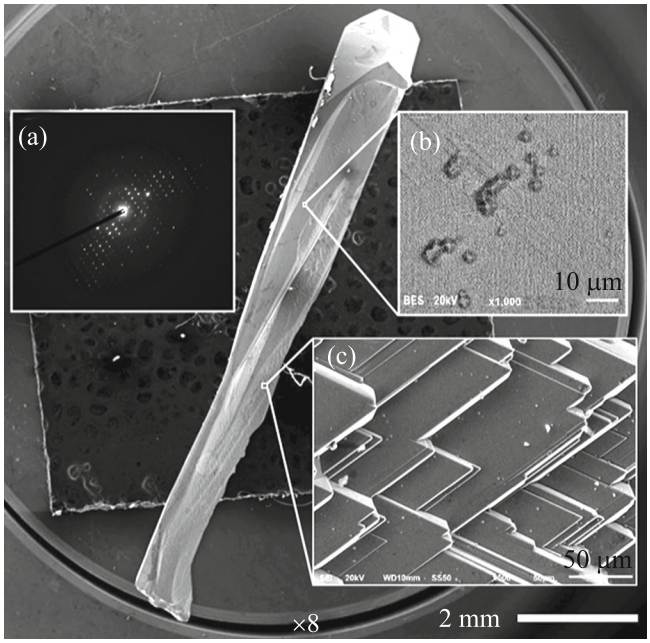

Fig. 1. Scanning electron microscopy image of a $(Cd_{0.993}Zn_{0.007})_3As_2$ sample. Inset (a) shows the electron diffraction image. Insets (b, c) show the magnified parts of its surface containing (b) growth nuclei and (c) cleavage planes.

gle crystals [5, 18], and we observed corresponding cleavage planes on the surface of studied $(Cd_{0.993}Zn_{0.007})_3As_2$ single crystal as shown in Fig. 1c.

In the Raman spectrum of the sample plotted in Fig. 2, we observed two clearly pronounced peaks at 194 and 249 cm^{-1}, and a weak peak at 292 cm^{-1}. Similar patterns were observed for micro- and nanocrystals, as well as for single crystalline thin films of Cd_3As_2 at room temperature [19–22]. In α-Cd_3As_2, the Raman vibrational spectrum is described by irreducible representations of the $I4_1cd$ space group, namely, by $\Gamma_R = 26A_1 + 27B_1 + 27B_2 + 65E$. Thus, the Raman spectrum must contain 145 active modes. Only 44 of them have been observed so far, with the maximum wavenumber of 221.8 cm^{-1} [23]. A detailed study of the Cd_3As_2 Raman spectra at different temperatures demonstrated that six strongest oscillators (B_{1g} modes) have wavenumbers within the 197.5–206.3 cm^{-1} range, and at high temperatures they may merge into one broad peak at about 190 cm^{-1} [23]. The 249 and 292 cm^{-1} peaks, which we observed, do not correspond to the main oscillations of the lattice, but they are characteristic of the Cd_3As_2. The nature of the peaks is still not quite clear. It is usually associated with the presence of the defects (Cd vacancies) and with the scattering of individual phonons and collective plasmon modes by the Dirac electron system [23].

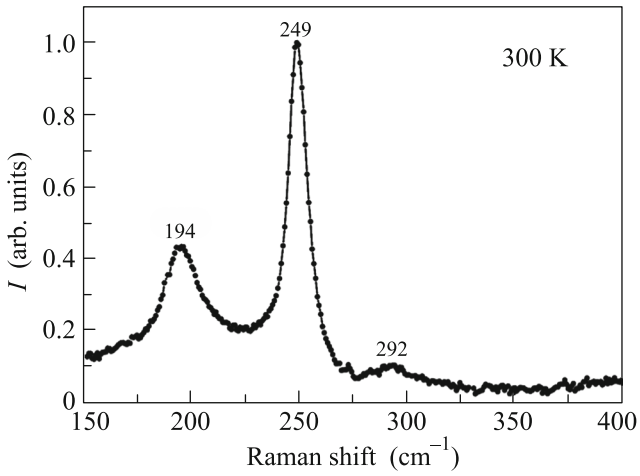

Fig. 2. Raman spectrum of the $(Cd_{0.993}Zn_{0.007})_3As_2$ sample measured at room temperature.

Magnetoresistance (MR) was measured at temperature $T = 4.2$ K for different magnetic field orientations and shown in Fig. 3. We observed clear SdH oscillations. The background part of the transverse MR ($R(B_\perp)$) is linear for $B > 1$ T and rather huge (more than 150%/T). The planar MR is nonlinear and is about a half of the transverse MR (see Fig. 3a).

In a trivial case, linear MR (LMR) can be explained in three different ways: (i) by the existence of the open Fermi surface (Kapitza model); (ii) by the transition to the ultraquantum limit (Abrikosov model [24]); and (iii) due to strong crystal inhomogeneity (Parish–Littlewood model [25]). Calculations and the experimental data show that in the undoped Cd_3As_2 with low carrier concentrations (less than 10^{18} cm^{-3}) the Fermi surface consists from two nearly spherical closed ellipsoids [26]. In our case, the Abrikosov model seems to be also irrelevant, because the observed LMR appears in magnetic fields substantially lower than the onset of SdH oscillations, while the number of observed oscillations suggest that LMR develops well below the ultraquantum limit. As shown previously, crystals under study demonstrate high crystalline quality, thus, confirming the absence of strong crystal inhomogeneity. From the other hand, LMR in Cd_3As_2 crystals can appear due to weak inhomogeneities (e.g., As vacancies) leading to the fluctuations of carrier mobilities [27]. This model is qualitatively similar to the Parish–Littlewood model, suggesting that such LMR should demonstrate only weak anisotropy. Thus, the observed substantial anisotropy of MR is, most probably, due to a chiral anomaly, resulting in negative MR contribution [28].

The SdH oscillations also reveal pronounced anisotropy. Corresponding oscillations for the $B_\perp$ demonstrate only a single frequency (Fig. 3b), while oscillations for $B_\parallel$ reveal more complicated behavior

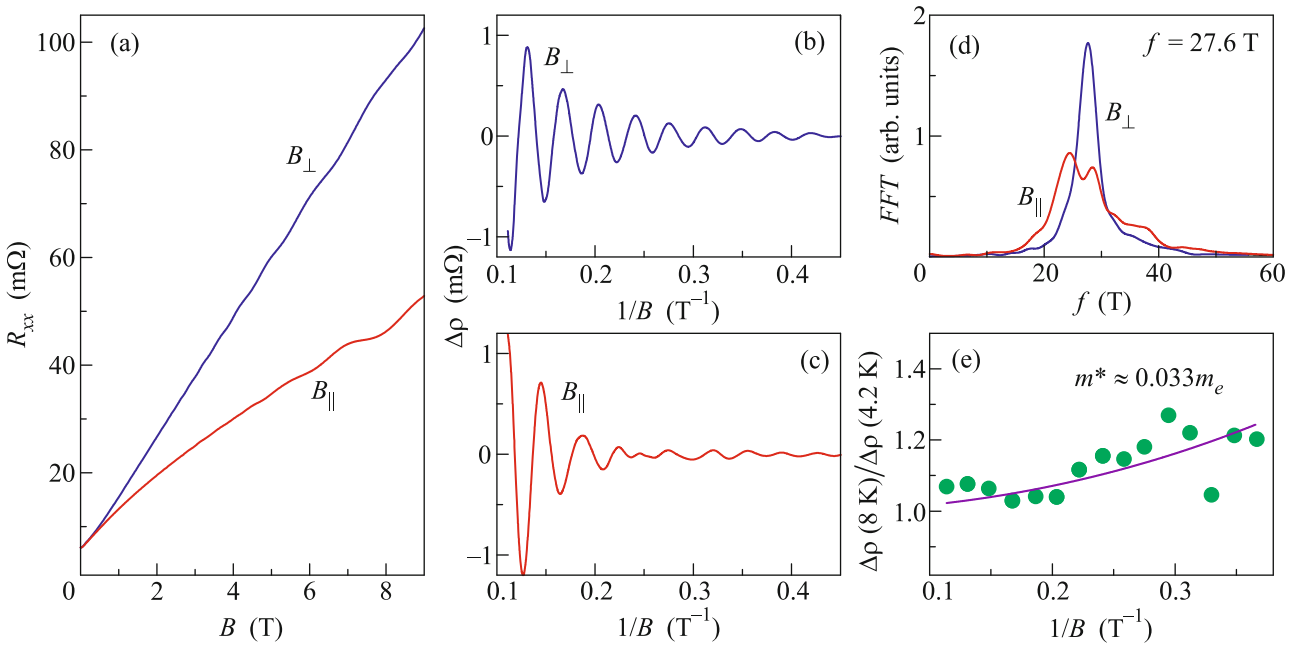

Fig. 3. (Color online) (a) Magnetoresistance curves for the $(Cd_{0.993}Zn_{0.007})_3As_2$ sample measured at 4.2 K for different magnetic field orientations. (b, c) Shubnikov–de Haas oscillations observed for (b) $B_\perp$ and (c) $B_\parallel$. (d) Corresponding Fourier spectra. (e) Ratio of SdH oscillation amplitudes measured for $B_\perp$ at 4.2 and 8 K; points show experimental data, the line shows the approximation by Eq. (1).

(Fig. 3c). The latter is related to the presence of two oscillation frequencies as it is suggested by corresponding Fourier spectra (Fig. 3d). A similar anisotropy of the SdH oscillations was observed for undoped Cd_3As_2 single crystals [26]. In [26], this behavior was attributed to a possible nesting of the Fermi-surface ellipsoids at some crystallographic directions.

The effective mass m^* of charge carriers in the investigated $(Cd_{0.993}Zn_{0.007})_3As_2$ single crystal was determined from the temperature dependence of the SdH oscillation amplitudes. Corresponding amplitudes increase when the temperature decreases. The relation between oscillation amplitudes $\Delta\rho(T_1)$ and $\Delta\rho(T_2)$ measured at temperatures T_1 and T_2 ($T_1 > T_2$) for the same value of the magnetic field $B = B_n$ (in the case of Dingle temperature being independent of temperature) is equal to [29]:

$$\frac{\Delta\rho(T_2)}{\Delta\rho(T_1)} = \frac{T_2}{T_1}\frac{\sinh\left(\frac{2\pi^2 k_B T_1}{\hbar\omega_c}\right)}{\sinh\left(\frac{2\pi^2 k_B T_2}{\hbar\omega_c}\right)}, \quad (1)$$

where $\omega_c = eB/m^*$ is the cyclotron frequency. Using Eq. (1) for $T_1 = 8$ K and $T_2 = 4.2$ K (see Fig. 3e), we evaluated $m^* \approx 0.033 m_e$ (m_e is the free electron mass). This value is in good agreement with $m^* \approx (0.023–0.043) m_e$ found for undoped Cd_3As_2 crystals [27].

The Fermi surface volume, V_F, determined from the SdH oscillations can be recalculated into carrier density according to the relation

$$n_{SdH} = \gamma\frac{V_F}{(2\pi\hbar)^3}, \quad (2)$$

where γ is the degeneracy factor. Usually only a spin degeneracy is taken into account, that is $\gamma = 2$. In the case of Cd_3As_2 it is assumed that there are two ellipsoids of the Fermi surface. Each of them is chiral-degenerate, that is $\gamma = 4$. Our experimental data suggest that the frequency of the SdH oscillations does not depend on the magnetic field orientation apart from the splitting (see Fig. 3d). This suggests that Fermi surfaces are nearly spherical. Thus, using Eq. (2) with $\gamma = 4$ we get $n_{SdH} \approx 1.6\times10^{18}$ cm^{-3}. Corresponding carrier mobility is about 5.5×10^4 cm^2/(V s).

The obtained results demonstrate the stability of the DSM phase in the Zn-doped Cd_3As_2 crystal. However, a substitution of Cd atoms by Zn (with lower atomic mass) may result in the modification of spin–orbit interaction amplitude, which affects the properties of DSM system. This motivates further studies of $(Cd_{1-x}Zn_x)_3As_2$ compound.

Needle-like $(Cd_{1-x}Zn_x)_3As_2$ single crystals were grown by the vapor-phase synthesis route. Structural

properties and low-temperature magnetoresistance of the $(Cd_{0.993}Zn_{0.007})_3As_2$ single crystal were investigated. Electron microscopy, electron diffraction, and Raman spectroscopy data confirm high crystalline perfection of the synthesized single crystal. Giant anisotropic magnetoresistance and Shubnikov–de Haas oscillations were observed at low temperatures. The experimental results indicate the presence of Dirac semimetal phase in $(Cd_{1-x}Zn_x)_3As_2$ with low zinc content.

This work was partially supported by the Russian Science Foundation (project no. 17-12-01345). Raman spectroscopy studies, performed by A.P. Kuzmenko and N.A. Khokhlov, were partially supported by the Ministry of Education and Science of the Russian Federation (project no. 16.2814.2017/PCh).

REFERENCES

1. N. P. Armitage, E. J. Mele, and A. Vishwanath, Rev. Mod. Phys. **90**, 015001 (2018).
2. L. P. He, X. C. Hong, J. K. Dong, J. Pan, Z. Zhang, J. Zhang, and S. Y. Li, Phys. Rev. Lett. **113**, 246402 (2014).
3. J. Feng, Y. Pang, D. Wu, Z. Wang, H. Weng, J. Li, X. Dai, Z. Fang, Y. Shi, and L. Lu, Phys. Rev. B **92**, 081306(R) (2015).
4. K. Zhang, H. Pan, M. Zhang, Z. Wei, M. Gao, F. Song, X. Wang, and R. Zhang, RSC Adv. **7**, 17689 (2017).
5. C.-Z. Li, R. Zhu, X. Ke, J.-M. Zhang, L. X. Wang, L. Zhang, Z.-M. Liao, and D.-P. Yu, Cryst. Growth Des. **15**, 3264 (2015).
6. A. V. Galeeva, I. V. Krylov, K. A. Drozdov, A. F. Knjazev, A. V. Kochura, A. P. Kuzmenko, V. S. Zakhvalinskii, S. N. Danilov, L. I. Ryabova, and D. R. Khokhlov, Belstein J. Nanotechnol. **8**, 167 (2017).
7. Q. Wang, C.-Z. Li, S. Ge, J.-G. Li, W. Lu, J. Lai, X. Liu, J. Ma, D.-P. Yu, Z.-M. Liao, and D. Sun, Nano Lett. **17**, 834 (2017).
8. J. Walowski and M. Munzenberg, J. Appl. Phys. **120**, 140901 (2016).
9. E. K. Arushanov, Prog. Cryst. Growth Charact. **3**, 211 (1981).
10. G. F. Volodina, V. S. Zakhvalinskii, and V. Kh. Kravtsov, Crystallogr. Rep. **58**, 563 (2013).
11. E. K. Arushanov, Prog. Cryst. Growth Charact. **25**, 131 (1992).
12. A. I. Belogorokhov, I. S. Zakharov, A. F. Knyazev, and A. V. Kochura, Inorg. Mater. **36**, 653 (2000).
13. T. Liang, Q. Gibson, M. N. Ali, M. Liu, R. J. Cava, and N. P. Ong, Nat. Mater. **14**, 280 (2015).
14. D. R. Lovett, *Semimetals and Narrow Band Semiconductors* (Pion, London, 1977).
15. E. K. Arushanov, A. F. Knyazev, A. N. Nateprov, and S. I. Radautsan, Sov. Phys. Semicond. **17**, 759 (1983).
16. H. Lu, X. Zhang, Y. Bian, and S. Jia, Sci. Rep. **7**, 3148 (2017).
17. R. Sankar, N. Neupane, S.-Y. Xu, et al., Sci. Rep. **5**, 12966 (2015).
18. M. N. Ali, Q. Gibson, S. Jeon, B. B. Zhou, A. Yazdani, and R. J. Cava, Inorg. Chem. **53**, 4062 (2014).
19. P. Schonher and T. Hesjedal, Appl. Phys. Lett. **106**, 013115 (2015).
20. K. Zhang, H. Pan, M. Zhang, Z. Wei, M. Gao, F. Song, X. Wang, and R. Zhang, RSC Adv. **7**, 17689 (2017).
21. P. Cheng, C. Zhang, Y. Liu, X. Yuan, F. Song, Q. Sun, P. Zhou, D. W. Zhang, and F. Xiu, New J. Phys. **18**, 083003 (2016).
22. A. V. Kochura, S. F. Marenkin, A. I. Ril, A. L. Zheludkevich, P. V. Abakumov, A. F. Knjazev, and M. B. Dobromyslov, J. Nano Electron. Phys. **7**, 04079 (2015).
23. A. Sharafeev, V. Gnezdilov, R. Sankar, F. C. Chou, and P. Lemmens, Phys. Rev. B **95**, 235148 (2017).
24. A. A. Abrikosov, J. Phys. A: Math. Gen. **36**, 9119 (2003).
25. M. M. Parish and P. B. Littlewood, Nature (London, U.K.) **426**, 162 (2003).
26. Y. Zhao, H. Liu, C. Zhang, H. Wang, J. Wang, Z. Lin, Y. Xing, H. Lu, J. Liu, Y. Wang, S. M. Brombosz, Z. Xiao, S. Jia, X. C. Xie, and J. Wang, Phys. Rev. X **5**, 031037 (2015).
27. A. Narayanan, M. D. Watson, S. F. Blake, N. Bruyant, L. Drigo, Y. L. Chen, D. Prabhakaran, B. Yan, C. Felser, T. Kong, P. C. Canfield, and A. I. Coldea, Phys. Rev. Lett. **114**, 117201 (2015).
28. H. Li, H. He, H.-Z. Lu, H. Zhang, H. Liu, R. Ma, Z. Fan, S.-Q. Shen, and J. Wang, Nat. Commun. **7**, 10301 (2016).
29. D. Shoenberg, *Magnetic Oscillations in Metals* (Cambridge Univ. Press, Cambridge, 1984).